Available online at www.eccomasproceedia.org
Eccomas Proceedia COMPDYN (2017) 1135-1154

ECCOMAS
Proceedia

COMPDYN 2017
6th ECCOMAS Thematic Conference on
Computational Methods in Structural Dynamics and Earthquake Engineering
M. Papadrakakis, M. Fragiadakis (eds.)
Rhodes Island, Greece, 15–17 June, 2017

TIME INTEGRATION OF DUAL CRAIG-BAMPTON REDUCED SYSTEMS

Fabian M. Gruber, Max Gille and Daniel J. Rixen

Chair of Applied Mechanics, Faculty of Mechanical Engineering, Technical University of Munich
Boltzmannstr. 15, 85748 Garching, Germany
e-mail: {fabian.gruber, max.gille, rixen}@tum.de

Keywords: Time Integration, Dynamic Substructuring, Component Mode Synthesis, Model Order Reduction, Dual Craig-Bampton Method.

Abstract. *In this paper, time integration procedures are demonstrated and investigated for dual Craig-Bampton reduced systems. The dual Craig-Bampton method for the reduction and successive coupling of dynamic systems employs free interface vibration modes, attachment modes and rigid body modes to build the reduction bases of the substructures, but assembles the substructures using interface forces. Thereby, the interface kinematic conditions are transformed, allowing for incompatibilities associated with the equilibrium residual in the substructure. Hence, the eigenvalues of the reduced-order model are not guaranteed to be upper bounds for the unreduced system's eigenvalues. Furthermore, the dual Craig-Bampton reduced system will always have as many negative eigenvalues as interface coupling conditions. The reduced system is unstable, rendering a straightforward time integration of the dual Craig-Bampton reduced system impossible.*

The feasibility of a reliable time integration of dual Craig-Bampton reduced systems is demonstrated and investigated in detail. The unstable behavior when time-integrating such systems without further modifications is illustrated and two approaches to overcome this instability are suggested: on the one hand, a modal analysis of the reduced system is performed as a subsequent step to the dual Craig-Bampton reduction. Only modes corresponding to positive eigenvalues are thereby kept for transient analysis. This allows for a stable time integration. On the other hand, a modal interface reduction during the dual Craig-Bampton reduction process is performed and only interface modes corresponding to positive eigenvalues are kept. This makes the final reduced system also positive definite. The accuracy using these two approaches is demonstrated in examples with either different initial conditions or varying external periodic excitations.

Peer-review under responsibility of the organizing committee of COMPDYN 2017.
doi: 10.7712/120117.5481.17213

1 INTRODUCTION

The increasing performance of modern computers makes it possible to solve very large linear systems of millions of degrees of freedom (DOFs) very fast. Nevertheless, since the refinement of finite element models is increasing faster than the computing capabilities, dynamic substructuring is still an essential tool for analyzing dynamical systems in an efficient manner. Building reduced models of submodels of a structure allows for the sharing of models between design groups. Moreover, the reduction of the DOFs of substructures is also important for building reduced order models for optimization and control. If a single component of a system is changed, only that component needs to be reanalyzed and the system can be analyzed at low additional cost. Thus, dynamic substructuring offers a flexible and efficient approach to dynamic analysis [1, 2, 3, 4, 5, 6, 7, 8, 9].

Dynamic substructuring techniques reduce the size of large models very efficiently. The large model is thereby divided into a certain number N of substructures; each substructure is analyzed and reduced separately and then assembled into a low-order reduced model. This low-order reduced model approximates the original large model's behavior. The most popular approach is a fixed interface method, the Craig-Bampton method (CBM) [1], which is based on fixed interface vibration modes and constraint modes. The substructures are assembled using interface displacements, which is referred to as primal assembly. Many other methods, such as those of MacNeal [2], Rubin [3], and Craig-Chang [4], employ free interface vibration modes, (residual) attachment modes, and rigid body modes and assemble the substructures in primal fashion as well. The dual Craig-Bampton method (DCBM) [6] also employs free interface vibration modes, (residual) attachment modes, and rigid body modes to build the substructures' reduction bases, but uses interface forces to assemble the substructures, which is referred to as dual assembly. As a consequence, the DCBM enforces only weak interface compatibility between the substructures. Thereby, interface locking problems are avoided as sometimes experienced in the primal assembly approaches [6]. Furthermore, the dual Craig-Bampton method leads to simpler reduced matrices compared to other free interface methods and preserves sparsity of the reduced matrices similar to the classical Craig-Bampton matrices [6]. Comparing the approximation accuracy of the lowest eigenvalues, the DCBM outperforms the CBM using the same number of normal modes per substructure as a reduction basis with comparable computational effort [9].

But, the dual Craig-Bampton reduced system will always have as many non-physical negative eigenvalues as interface coupling conditions due to the weak interface compatibility between the substructures. If a very small reduction basis is used for the substructures (using only a very small number of free interface vibration modes), the negative eigenvalues of the reduced problem show up in the low frequency range [10]. If the reduction basis is large enough, the negative eigenvalues are shifted in the high frequency range and do not show up if only the lowest eigenvalues of the original system are approximated [6], which is commonly the case. These negative eigenvalues are related to the weak compatibility of the interfaces and are not meaningful from a physical point of view. Nevertheless, the non-physical negative eigenvalues of the reduced dually assembled problem are intrinsic in the reduction process using the DCBM [6].

Thus, when applying a DCBM reduction, the reduced system is not positive definite anymore. This means that the reduced system is unstable, rendering a straightforward time integration of the DCBM reduced system impossible. The instability is demonstrated by way of example in Figure 1. Figure 1a shows a static displacement of a two-dimensional structure decomposed into two substructures (this example will be examined in detail in section 4). A

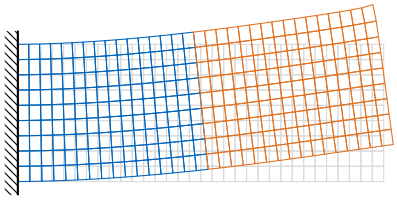

(a) Static initial displacement of a two-dimensional solid problem decomposed into two substructures. The displacement is due to a vertical static force f_0 on the upper-right corner (see Figure 3a). Both substructures are respectively discretized by 16×9 bilinear four-noded elements (plane stress) and the structure is clamped on the left side in both directions.

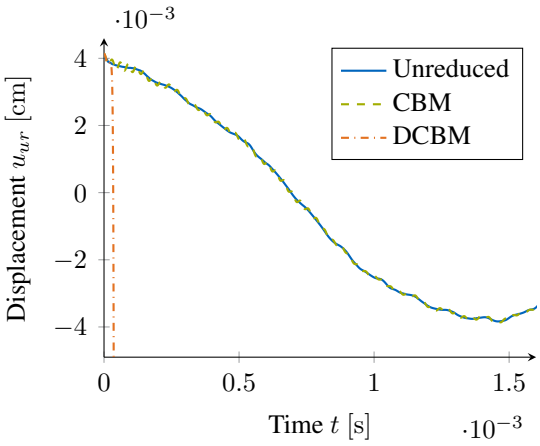

(b) Vertical displacement u_{ur} of the upper-right corner for unreduced, CBM reduced and DCBM reduced structures.

Figure 1: Instability of dual Craig-Bampton reduced (DCBM) system after static initial displacement. The unreduced system (Unreduced), the Craig-Bampton reduced system (CBM) and the dual Craig-Bampton reduced system (DCBM) are prestressed with the same initial displacement. The DCBM reduced system becomes immediately unstable and diverges after a few time steps ($t < 0.1 \cdot 10^{-3}\,\mathrm{s}$).

Craig-Bampton (CBM) and a dual Craig-Bampton (DCBM) reduction are respectively applied to the structure and the reduced systems are used without any modification for time integration. The initially prestressed structure of Figure 1a is released and the vertical displacement u_{ur} of the upper-right corner is considered. Figure 1b compares the vertical displacement u_{ur} of the upper-right corner for the unreduced system, the CBM reduced system and the DCBM reduced system. The DCBM reduced system becomes immediately unstable and diverges after a few time steps (for $t < 0.1 \cdot 10^{-3}\,\mathrm{s}$ in Figure 1b). This unstable behavior is a result of the negative eigenvalues in the DCBM reduced system. Therefore, direct time integration of a DCBM reduced system is impossible.

The feasibility of a reliable time integration of DCBM reduced systems is demonstrated and investigated in detail in this contribution. Two possible approaches to overcome the instability will be presented that allow for a stable time integration. On the one hand, a modal analysis of the reduced system is performed as a subsequent step to the DCBM reduction. On the other hand, a modal interface reduction during the DCBM reduction process is performed. The accuracy of the time integration of these two approaches is illustrated by different examples. Free vibration with different initial conditions or varying external periodic excitations are considered.

In section 2, the original formulation of the dual Craig-Bampton method for undamped systems is concisely surveyed. Common time integration schemes are recalled. The terminology and notations used throughout this paper are outlined. Following this, strategies to simulate a dual Craig-Bampton reduced system are derived in section 3. The properties of the proposed strategies are subsequently illustrated in detail by way of example in section 4. Section 5 tries to provide some recommendations for the reliable time integration of dual Craig-Bampton reduced systems. Finally a brief summary of findings and conclusions is given in section 6.

2 GOVERNING EQUATIONS

2.1 Dual Craig-Bampton method

In this section, we briefly summarize the dual Craig-Bampton method (DCBM) for undamped structures [6]. Consider a domain that is divided into N non-overlapping substructures such that every node belongs to exactly one substructure except for the nodes on the interface boundaries. The equation of motion of one undamped substructure s is

$$\boldsymbol{M}^{(s)}\ddot{\boldsymbol{u}}^{(s)} + \boldsymbol{K}^{(s)}\boldsymbol{u}^{(s)} = \boldsymbol{f}^{(s)} + \boldsymbol{g}^{(s)}, \qquad s = 1, \dots, N. \tag{1}$$

The superscript (s) is the label of the particular substructure s. $\boldsymbol{M}^{(s)}$, $\boldsymbol{K}^{(s)}$, and $\boldsymbol{u}^{(s)}$ are respectively the substructure's mass matrix, stiffness matrix, and displacement vector. $\boldsymbol{f}^{(s)}$ is the external force vector and $\boldsymbol{g}^{(s)}$ is the vector of reaction forces on the substructure due to its connection to adjacent substructures at its boundary DOF.

2.1.1 Dual assembly

One way to enforce the interface compatibility between the different substructures is to consider the interface connecting forces $\boldsymbol{g}^{(s)}$ as unknowns. These forces must be determined to satisfy the interface compatibility condition (displacement equality) and the local equation of motion of the substructures:

$$\sum_{s=1}^{N} \boldsymbol{B}^{(s)}\boldsymbol{u}^{(s)} = \boldsymbol{0} \tag{2}$$

$$\boldsymbol{M}^{(s)}\ddot{\boldsymbol{u}}^{(s)} + \boldsymbol{K}^{(s)}\boldsymbol{u}^{(s)} + \boldsymbol{B}^{(s)^T}\boldsymbol{\lambda} = \boldsymbol{f}^{(s)}, \qquad s = 1, \dots, N \tag{3}$$

$\boldsymbol{B}^{(s)}$ is a signed Boolean matrix acting on substructure DOFs $\boldsymbol{u}^{(s)}$, which is a submatrix of the constraint matrix $\boldsymbol{B}$ which will be defined below in Eq. (6). Vector $\boldsymbol{B}^{(s)^T}\boldsymbol{\lambda}$ represents the interconnecting forces between substructures, which corresponds to the negative interface reaction force vector $\boldsymbol{g}^{(s)}$ in Eq. (1). This means

$$\boldsymbol{g}^{(s)} = -\boldsymbol{B}^{(s)^T}\boldsymbol{\lambda}. \tag{4}$$

$\boldsymbol{\lambda}$ is the vector of all Lagrange multipliers acting on the interfaces that are the additional unknowns. Using the block-diagonal matrices

$$\boldsymbol{M}_{\text{bd}} = \begin{bmatrix} \boldsymbol{M}^{(1)} & & \boldsymbol{0} \\ & \ddots & \\ \boldsymbol{0} & & \boldsymbol{M}^{(N)} \end{bmatrix}, \quad \boldsymbol{K}_{\text{bd}} = \begin{bmatrix} \boldsymbol{K}^{(1)} & & \boldsymbol{0} \\ & \ddots & \\ \boldsymbol{0} & & \boldsymbol{K}^{(N)} \end{bmatrix}, \tag{5}$$

and the corresponding partitioned vectors and Boolean matrix

$$\boldsymbol{u} = \begin{bmatrix} \boldsymbol{u}^{(1)} \\ \vdots \\ \boldsymbol{u}^{(N)} \end{bmatrix}, \quad \boldsymbol{f} = \begin{bmatrix} \boldsymbol{f}^{(1)} \\ \vdots \\ \boldsymbol{f}^{(N)} \end{bmatrix}, \quad \boldsymbol{B} = \begin{bmatrix} \boldsymbol{B}^{(1)} & \cdots & \boldsymbol{B}^{(N)} \end{bmatrix}, \tag{6}$$

substructure Eqs. (2) and (3) can be assembled as

$$\begin{bmatrix} \boldsymbol{M}_{\text{bd}} & \boldsymbol{0} \\ \boldsymbol{0} & \boldsymbol{0} \end{bmatrix} \begin{bmatrix} \ddot{\boldsymbol{u}} \\ \ddot{\boldsymbol{\lambda}} \end{bmatrix} + \begin{bmatrix} \boldsymbol{K}_{\text{bd}} & \boldsymbol{B}^T \\ \boldsymbol{B} & \boldsymbol{0} \end{bmatrix} \begin{bmatrix} \boldsymbol{u} \\ \boldsymbol{\lambda} \end{bmatrix} = \begin{bmatrix} \boldsymbol{f} \\ \boldsymbol{0} \end{bmatrix}. \tag{7}$$

$\boldsymbol{B}$ is referred to as the constraint matrix [7]. In this hybrid formulation, the Lagrange multipliers $\boldsymbol{\lambda}$ enforce the interface compatibility constraints and can be identified as interface forces [6].

2.1.2 Reduction of dual assembled system

Considering the equation of motion (3) of substructure s, every substructure can be seen as being excited by the interface connection forces $\boldsymbol{\lambda}$. This indicates that the local dynamic behavior can be described by superposing local static and local dynamic modes. The displacements $\boldsymbol{u}^{(s)}$ of each substructure are expressed in terms of local static solutions $\boldsymbol{u}_{\text{stat}}^{(s)}$ and in terms of eigenmodes associated with the entire substructure matrices $\boldsymbol{K}^{(s)}$ and $\boldsymbol{M}^{(s)}$:

$$\boldsymbol{u}^{(s)} = \boldsymbol{u}_{\text{stat}}^{(s)} + \sum_{j=1}^{n^{(s)}-r^{(s)}} \boldsymbol{\theta}_j^{(s)} \eta_j^{(s)} \qquad \text{with} \qquad \boldsymbol{u}_{\text{stat}}^{(s)} = -\boldsymbol{K}^{(s)^+} \boldsymbol{B}^{(s)^T} \boldsymbol{\lambda} + \sum_{j=1}^{r^{(s)}} \boldsymbol{R}_j^{(s)} \alpha_j^{(s)} \tag{8}$$

$n^{(s)}$ is the dimension of the local substructure problem. Matrix $\boldsymbol{K}^{(s)^+}$ is equal to the inverse of $\boldsymbol{K}^{(s)}$ if there are enough boundary conditions to prevent the substructure from floating when its interface with adjacent substructures is free [6]. If a substructure is floating, then the generalized inverse $\boldsymbol{K}^{(s)^+}$ has to be used. $\boldsymbol{R}^{(s)}$ is the matrix containing the $n_r^{(s)}$ rigid body modes as columns that are orthonormalized with respect to the mass matrix $\boldsymbol{M}^{(s)}$. Vector $\boldsymbol{\alpha}^{(s)}$ contains the amplitudes $\alpha_j^{(s)}$ of the rigid body modes $\boldsymbol{R}_j^{(s)}$. The flexibility matrix $\boldsymbol{G}^{(s)}$ in inertia-relief format is computed from any generalized inverse $\boldsymbol{K}^{(s)^+}$ by projecting out the rigid body modes $\boldsymbol{R}^{(s)}$ using the inertia-relief projection matrix $\boldsymbol{P}^{(s)}$ which is defined as [7, 11]

$$\boldsymbol{P}^{(s)} = \boldsymbol{I}^{(s)} - \boldsymbol{M}^{(s)} \boldsymbol{R}^{(s)} \boldsymbol{R}^{(s)^T} \tag{9}$$

and therefore

$$\boldsymbol{G}^{(s)} = \boldsymbol{P}^{(s)^T} \boldsymbol{K}^{(s)^+} \boldsymbol{P}^{(s)}. \tag{10}$$

Vector $\boldsymbol{\eta}^{(s)}$ contains the amplitudes $\eta_j^{(s)}$ of the local eigenmodes $\boldsymbol{\theta}_j^{(s)}$ being eigensolutions of the generalized eigenproblem

$$\left(-\omega_j^{(s)^2} \boldsymbol{M}^{(s)} + \boldsymbol{K}^{(s)}\right) \boldsymbol{\theta}_j^{(s)} = \boldsymbol{0}. \tag{11}$$

These free interface normal modes $\boldsymbol{\theta}_j^{(s)}$ are also orthonormalized with respect to the mass matrix $\boldsymbol{M}^{(s)}$. An approximation is obtained by retaining only the first free interface normal modes $\boldsymbol{\theta}_j^{(s)}$ corresponding to the $n_\theta^{(s)}$ lowest eigenvalues $\omega_j^{(s)^2}$ of Eq. (11). Calling $\boldsymbol{\Theta}_{n_\theta}^{(s)}$ the matrix containing these eigenmodes as columns, the approximation of the displacements $\boldsymbol{u}^{(s)}$ of the substructure is given by

$$\boldsymbol{u}^{(s)} \approx -\boldsymbol{G}^{(s)} \boldsymbol{B}^{(s)^T} \boldsymbol{\lambda} + \boldsymbol{R}^{(s)} \boldsymbol{\alpha}^{(s)} + \boldsymbol{\Theta}_{n_\theta}^{(s)} \boldsymbol{\eta}^{(s)}. \tag{12}$$

Matrix $\boldsymbol{\Theta}_{n_\theta}^{(s)}$ of kept eigenmodes satisfies

$$\boldsymbol{\Theta}_{n_\theta}^{(s)^T} \boldsymbol{K}^{(s)} \boldsymbol{\Theta}_{n_\theta}^{(s)} = \boldsymbol{\Omega}^{(s)^2} = \text{diag}\left(\omega_1^{(s)^2}, \ldots, \omega_{n_\theta}^{(s)^2}\right) \qquad \text{and} \qquad \boldsymbol{\Theta}_{n_\theta}^{(s)^T} \boldsymbol{M}^{(s)} \boldsymbol{\Theta}_{n_\theta}^{(s)} = \boldsymbol{I} \tag{13}$$

with $\boldsymbol{\Omega}^{(s)}$ being a diagonal matrix containing the $n_\theta^{(s)}$ kept eigenvalues $\omega_j^{(s)}$. Since a part of the subspace spanned by $\boldsymbol{\Theta}_{n_\theta}^{(s)}$ is already included in $\boldsymbol{G}^{(s)}$, residual flexibility matrix $\boldsymbol{G}_{\text{res}}^{(s)}$ can be used instead of flexibility matrix $\boldsymbol{G}^{(s)}$. The residual flexibility matrix $\boldsymbol{G}_{\text{res}}^{(s)}$ is defined by

$$\boldsymbol{G}_{\text{res}}^{(s)} = \sum_{j=n_\theta^{(s)}+1}^{n^{(s)}-n_r^{(s)}} \frac{\boldsymbol{\theta}_j^{(s)} \boldsymbol{\theta}_j^{(s)^T}}{\omega_j^{(s)^2}} = \boldsymbol{G}^{(s)} - \sum_{j=1}^{n_\theta^{(s)}} \frac{\boldsymbol{\theta}_j^{(s)} \boldsymbol{\theta}_j^{(s)^T}}{\omega_j^{(s)^2}}. \tag{14}$$

Note that $\boldsymbol{G}_{\text{res}}^{(s)} = \boldsymbol{G}_{\text{res}}^{(s)^T}$, which is computed using the second equality in Eq. (14). For further properties of $\boldsymbol{G}_{\text{res}}^{(s)}$ see [6, 12]. As a result, the approximation of one substructure is

$$\boldsymbol{u}^{(s)} \approx -\boldsymbol{G}_{\text{res}}^{(s)}\boldsymbol{B}^{(s)^T}\boldsymbol{\lambda} + \boldsymbol{R}^{(s)}\boldsymbol{\alpha}^{(s)} + \boldsymbol{\Theta}_{n_\theta}^{(s)}\boldsymbol{\eta}^{(s)} = \begin{bmatrix} \boldsymbol{R}^{(s)} & \boldsymbol{\Theta}_{n_\theta}^{(s)} & -\boldsymbol{G}_{\text{res}}^{(s)}\boldsymbol{B}^{(s)^T} \end{bmatrix} \begin{bmatrix} \boldsymbol{\alpha}^{(s)} \\ \boldsymbol{\eta}^{(s)} \\ \boldsymbol{\lambda} \end{bmatrix}. \quad (15)$$

Assembling all N substructures in a dual fashion according to Eq. (7) by keeping the interface forces $\boldsymbol{\lambda}$ as unknowns, the entire structure can consequently be approximated by

$$\begin{bmatrix} \boldsymbol{u} \\ \boldsymbol{\lambda} \end{bmatrix} \approx \underbrace{\begin{bmatrix} \boldsymbol{R}^{(1)} & \boldsymbol{\Theta}_{n_\theta}^{(1)} & & & \boldsymbol{0} & \boldsymbol{0} & -\boldsymbol{G}_{\text{res}}^{(1)}\boldsymbol{B}^{(1)^T} \\ & & \ddots & \ddots & & & \vdots \\ \boldsymbol{0} & \boldsymbol{0} & & & \boldsymbol{R}^{(N)} & \boldsymbol{\Theta}_{n_\theta}^{(N)} & -\boldsymbol{G}_{\text{res}}^{(N)}\boldsymbol{B}^{(N)^T} \\ \boldsymbol{0} & \boldsymbol{0} & & & \boldsymbol{0} & \boldsymbol{0} & \boldsymbol{I} \end{bmatrix}}_{\boldsymbol{T}_{\text{DCB}}} \begin{bmatrix} \boldsymbol{\alpha}^{(1)} \\ \boldsymbol{\eta}^{(1)} \\ \vdots \\ \boldsymbol{\alpha}^{(N)} \\ \boldsymbol{\eta}^{(N)} \\ \boldsymbol{\lambda} \end{bmatrix}. \quad (16)$$

The approximation of the dually assembled system's dynamic equations (7) is

$$\begin{aligned} &\boldsymbol{M}_{\text{DCB}} \begin{bmatrix} \ddot{\boldsymbol{\alpha}}^{(1)} \\ \ddot{\boldsymbol{\eta}}^{(1)} \\ \vdots \\ \ddot{\boldsymbol{\alpha}}^{(N)} \\ \ddot{\boldsymbol{\eta}}^{(N)} \\ \ddot{\boldsymbol{\lambda}} \end{bmatrix} + \boldsymbol{K}_{\text{DCB}} \begin{bmatrix} \boldsymbol{\alpha}^{(1)} \\ \boldsymbol{\eta}^{(1)} \\ \vdots \\ \boldsymbol{\alpha}^{(N)} \\ \boldsymbol{\eta}^{(N)} \\ \boldsymbol{\lambda} \end{bmatrix} = \boldsymbol{f}_{\text{DCB}} \\ \text{with} \quad &\boldsymbol{M}_{\text{DCB}} = \boldsymbol{T}_{\text{DCB}}^T \begin{bmatrix} \boldsymbol{M}_{\text{bd}} & \boldsymbol{0} \\ \boldsymbol{0} & \boldsymbol{0} \end{bmatrix} \boldsymbol{T}_{\text{DCB}}, \\ &\boldsymbol{K}_{\text{DCB}} = \boldsymbol{T}_{\text{DCB}}^T \begin{bmatrix} \boldsymbol{K}_{\text{bd}} & \boldsymbol{B}^T \\ \boldsymbol{B} & \boldsymbol{0} \end{bmatrix} \boldsymbol{T}_{\text{DCB}}, \qquad \boldsymbol{f}_{\text{DCB}} = \boldsymbol{T}_{\text{DCB}}^T \begin{bmatrix} \boldsymbol{f} \\ \boldsymbol{0} \end{bmatrix}. \end{aligned} \quad (17)$$

The dual Craig-Bampton reduced system is quasi-diagonal (similar to the reduced matrices of the Craig-Bampton method [1]) and has the final size of $n_{\text{DCB}} = \sum_{s=1}^{N} n_r^{(s)} + \sum_{s=1}^{N} n_\theta^{(s)} + n_\lambda$ with $n_r^{(s)}$ rigid body modes of substructure s, with $n_\theta^{(s)}$ kept free interface normal modes of substructure s, and with the total number n_λ of all Lagrange multipliers [6, 9].

2.1.3 Modal truncation vectors related to external force excitations

Consider the case in which a structure is loaded by an external force $\boldsymbol{f}$ with force application point not being an interface DOF. As introduced in the previous section, the DCBM reduced system is not able to represent the static deformation $\boldsymbol{u}_0$ due to this force $\boldsymbol{f}$ correctly. The correct static deformation $\boldsymbol{u}_0$ due to this force $\boldsymbol{f}$ can be computed via the inverse of the unreduced stiffness matrix:

$$\boldsymbol{u}_0 = \boldsymbol{K}^{-1}\boldsymbol{f}$$

If the force $\boldsymbol{f}$ is not applied at one of the interface DOFs, the subspace spanned by the reduction basis $\boldsymbol{T}_{\text{DCB}}$ of the DCBM system does not include this static displacement $\boldsymbol{u}_0$. If we want to

compute the structure's correct static response $\boldsymbol{u}_0$ due to the external force $\boldsymbol{f}$, we need to enrich the reduction basis in such a way that:

$$\boldsymbol{u}_0 \in \text{colspan}(\boldsymbol{T}_{\text{DCB}}) \tag{18}$$

The columns of the basis $\boldsymbol{T}_{\text{DCB}}$ have to span a space that is able to represent the static displacement $\boldsymbol{u}_0$. This is easily achieved by adding an additional attachment mode $\boldsymbol{\psi}_a$ corresponding to the external force $\boldsymbol{f}$ to the reduction basis $\boldsymbol{T}_{\text{DCB}}$. Such an additional attachment mode $\boldsymbol{\psi}_a$ is often called a load dependent Ritz vector [13, 14, 15] or modal truncation vector [16, 17]. For the case of a structure decomposed into two substructures and an external force $\boldsymbol{f}$ with force application point on substructure 2, the augmented reduction matrix of the dual Craig-Bampton method is:

$$\boldsymbol{T}_{\text{DCB,aug}} = \begin{bmatrix} \boldsymbol{R}^{(1)} & \boldsymbol{\Theta}^{(1)}_{n_\theta} & \boldsymbol{0} & \boldsymbol{0} & \boldsymbol{0} & -\boldsymbol{G}^{(1)}_{\text{res}} \boldsymbol{B}^{(1)^T} \\ \boldsymbol{0} & \boldsymbol{0} & \boldsymbol{R}^{(2)} & \boldsymbol{\Theta}^{(2)}_{n_\theta} & \boldsymbol{\psi}^{(2)}_a & -\boldsymbol{G}^{(2)}_{\text{res}} \boldsymbol{B}^{(2)^T} \\ \boldsymbol{0} & \boldsymbol{0} & \boldsymbol{0} & \boldsymbol{0} & \boldsymbol{0} & \boldsymbol{I} \end{bmatrix} \tag{19}$$

Thereby, the attachment mode $\boldsymbol{\psi}^{(2)}_a$ is associated with the force vector $\boldsymbol{f}^{(2)}$, which is the part of the external force vector $\boldsymbol{f}$ corresponding to substructure 2, and can be easily obtained as

$$\boldsymbol{\psi}^{(2)}_a = \boldsymbol{G}^{(2)}_{\text{res}} \boldsymbol{B}^{(2)^T}_f. \tag{20}$$

$\boldsymbol{B}^{(2)}_f$ is a Boolean matrix defining the force input DOFs. In contrast to the DCBM reduction basis of Eq. (16), the augmented basis $\boldsymbol{T}_{\text{DCB,aug}}$ can now represent any static deformation due to force $\boldsymbol{f}$.

2.2 Time integration

The time integration scheme used in this paper is the Newmark algorithm [18]. It introduces two parameters β and γ. The displacement $\boldsymbol{u}_{n+1}$ and velocity $\dot{\boldsymbol{u}}_{n+1}$ at time $t_{n+1} = t_n + h$ are expressed only depending on values of the previous time step t_n and the time step size h [18]:

$$\boldsymbol{u}_{n+1} = \boldsymbol{u}_n + \dot{\boldsymbol{u}}_n h + \left(\tfrac{1}{2} - \beta\right) \ddot{\boldsymbol{u}}_n h^2 + \beta \ddot{\boldsymbol{u}}_{n+1} h^2 \tag{21}$$

$$\dot{\boldsymbol{u}}_{n+1} = \dot{\boldsymbol{u}}_n + (1 - \gamma) \ddot{\boldsymbol{u}}_n h + \gamma \ddot{\boldsymbol{u}}_{n+1} h \tag{22}$$

Formulating the dynamic equilibrium at time t_{n+1}

$$\boldsymbol{M} \ddot{\boldsymbol{u}}_{n+1} = \boldsymbol{f}_{n+1} - \boldsymbol{C} \dot{\boldsymbol{u}}_{n+1} - \boldsymbol{K} \boldsymbol{u}_{n+1} \tag{23}$$

and inserting the expressions of Eqs. (21) and (22), the acceleration $\ddot{\boldsymbol{u}}_{n+1}$ at t_{n+1} can be determined:

$$\begin{aligned} \overbrace{\left[\boldsymbol{M} + h\gamma \boldsymbol{C} + h^2 \beta \boldsymbol{K}\right]}^{\boldsymbol{S}} \ddot{\boldsymbol{u}}_{n+1} = & - \boldsymbol{C} \left[\dot{\boldsymbol{u}}_n + (1 - \gamma) h \ddot{\boldsymbol{u}}_n\right] \\ & - \boldsymbol{K} \left[\boldsymbol{u}_n + h \dot{\boldsymbol{u}}_n + \left(\tfrac{1}{2} - \beta\right) h^2 \ddot{\boldsymbol{u}}_n\right] \\ & + \boldsymbol{f}\left(t_{n+1}\right). \end{aligned} \tag{24}$$

The time stepping matrix $\boldsymbol{S}$ is computed and factorized a priori if the time step size h is constant. This way, accelerations $\ddot{\boldsymbol{u}}_{n+1}$ at time t_{n+1} are obtained and displacements $\boldsymbol{u}_{n+1}$ and velocities $\dot{\boldsymbol{u}}_{n+1}$ directly result from Eqs. (21) and (22). A common choice [7, 11, 18] for the parameters is $\gamma = \frac{1}{2}$ and $\beta = \frac{1}{4}$, which are also used in this paper.

3 TIME INTEGRATION STRATEGIES

Two possibilities to eliminate the negative eigenvalues of DCBM reduced systems are proposed. Both methods are based on the idea of a second reduction of the reduced quantities $\boldsymbol{M}_{\text{red1}}$, $\boldsymbol{K}_{\text{red1}}$ and $\boldsymbol{f}_{\text{red1}}$, which are obtained by a first reduction, e.g., a CBM or DCBM reduction. The reduced equation of motion of the mechanical system after the first reduction is

$$\boldsymbol{M}_{\text{red1}}\ddot{\boldsymbol{u}}_{\text{red1}} + \boldsymbol{K}_{\text{red1}}\boldsymbol{u}_{\text{red1}} = \boldsymbol{f}_{\text{red1}} \tag{25}$$

with vector $\boldsymbol{u}_{\text{red1}}$ of reduced coordinates of size n_{red1}. Associated with the reduced system of Eq. (25) is the eigenvalue problem

$$\left(-\omega_j^2 \boldsymbol{M}_{\text{red1}} + \boldsymbol{K}_{\text{red1}}\right)\boldsymbol{x}_j = \boldsymbol{0} \tag{26}$$

with eigenvalue ω_j^2 and corresponding eigenvector $\boldsymbol{x}_j$ for $j = 1, \ldots, n_{\text{red1}}$. Eigenvectors $\boldsymbol{x}_j$ of Eq. (26) are called normal modes or natural modes and form the modal matrix

$$\boldsymbol{X}_{\text{modal}} = \begin{bmatrix}\boldsymbol{x}_1 & \boldsymbol{x}_2 & \ldots & \boldsymbol{x}_{n_{\text{red1}}}\end{bmatrix}. \tag{27}$$

If the modal matrix $\boldsymbol{X}_{\text{modal}}$ is normalized with respect to the mass matrix $\boldsymbol{M}_{\text{red1}}$, then the normal modes' orthogonality conditions give

$$\tilde{\boldsymbol{M}} = \boldsymbol{X}_{\text{modal}}^T \boldsymbol{M}_{\text{red1}} \boldsymbol{X}_{\text{modal}} = \boldsymbol{I} \tag{28}$$

$$\tilde{\boldsymbol{K}} = \boldsymbol{X}_{\text{modal}}^T \boldsymbol{K}_{\text{red1}} \boldsymbol{X}_{\text{modal}} = \text{diag}\left(\omega_1^2, \ldots, \omega_n^2\right). \tag{29}$$

Thereby $\tilde{\boldsymbol{M}}$ is the transformed mass matrix and $\tilde{\boldsymbol{K}}$ is the transformed stiffness matrix. The result of the modal transformation is a system of n_{red1} decoupled equations. This allows one to remove the negative eigenvalues ω_j^2 from the system by truncating the corresponding modes. In our case, the truncated modes will be those modes corresponding to negative eigenvalues of the DCBM reduced system. Therefore, a reduction matrix $\boldsymbol{T}_{\text{red2}}$ is used that contains only the eigenvectors $\boldsymbol{x}_j$ corresponding to positive eigenvalues ω_j^2. If this reduction matrix $\boldsymbol{T}_{\text{red2}}$ is used instead of the entire modal matrix $\boldsymbol{X}_{\text{modal}}$, Eqs. (28) and (29) become a further reduction. Then the reduced matrices $\boldsymbol{M}_{\text{red2}}$, $\boldsymbol{K}_{\text{red2}}$ and the reduced force vector $\boldsymbol{f}_{\text{red2}}$ after this second reduction are obtained:

$$\boldsymbol{M}_{\text{red2}} = \boldsymbol{T}_{\text{red2}}^T \boldsymbol{M}_{\text{red1}} \boldsymbol{T}_{\text{red2}}, \qquad \boldsymbol{K}_{\text{red2}} = \boldsymbol{T}_{\text{red2}}^T \boldsymbol{K}_{\text{red1}} \boldsymbol{T}_{\text{red2}}, \qquad \boldsymbol{f}_{\text{red2}} = \boldsymbol{T}_{\text{red2}}^T \boldsymbol{f}_{\text{red1}} \tag{30}$$

The corresponding equation of motion is

$$\boldsymbol{M}_{\text{red2}}\ddot{\boldsymbol{u}}_{\text{red2}} + \boldsymbol{K}_{\text{red2}}\boldsymbol{u}_{\text{red2}} = \boldsymbol{f}_{\text{red2}}. \tag{31}$$

Vector $\boldsymbol{u}_{\text{red2}}$ is the vector of reduced coordinates of size n_{red2} after the second reduction with basis $\boldsymbol{T}_{\text{red2}}$.

In the following, two possibilities are considered to construct this second reduction basis $\boldsymbol{T}_{\text{red2}}$ and therefore to eliminate the negative eigenvalues of DCBM reduced systems:

- Subsequent modal reduction of DCBM reduced system in section 3.1
- Subsequent modal interface reduction of DCBM reduced system in section 3.2

3.1 Modal reduction of dual Craig-Bampton reduced system

The DCBM reduced system of Eq. (17) is further reduced analogously to the reduction represented by Eq. (30) with $\boldsymbol{M}_{\text{red1}} = \boldsymbol{M}_{\text{DCB}}$, $\boldsymbol{K}_{\text{red1}} = \boldsymbol{K}_{\text{DCB}}$ and $\boldsymbol{f}_{\text{red1}} = \boldsymbol{f}_{\text{DCB}}$. That way, all positive eigenvalues of the unmodified DCBM reduced system are preserved in the process of removing the unphysical negative ones. In doing so, $\boldsymbol{T}_{\text{red2}}$ is the matrix containing the eigenvectors $\boldsymbol{x}_{\text{DCB},j}$ corresponding only to positive eigenvalues $\omega^2_{\text{DCB},j}$ of the eigenproblem

$$\left(-\omega^2_{\text{DCB},j}\boldsymbol{M}_{\text{DCB}} + \boldsymbol{K}_{\text{DCB}}\right)\boldsymbol{x}_{\text{DCB},j} = \boldsymbol{0}. \tag{32}$$

Then, the modified DCBM system is

$$\boldsymbol{M}_{\text{DCBmod}}\ddot{\boldsymbol{\eta}}_{\text{DCBmod}} + \boldsymbol{K}_{\text{DCBmod}}\boldsymbol{\eta}_{\text{DCBmod}} = \boldsymbol{f}_{\text{DCBmod}} \tag{33}$$

with

$$\boldsymbol{M}_{\text{DCBmod}} = \boldsymbol{T}^T_{\text{red2}}\boldsymbol{M}_{\text{DCB}}\boldsymbol{T}_{\text{red2}}, \quad \boldsymbol{K}_{\text{DCBmod}} = \boldsymbol{T}^T_{\text{red2}}\boldsymbol{K}_{\text{DCB}}\boldsymbol{T}_{\text{red2}}, \quad \boldsymbol{f}_{\text{DCBmod}} = \boldsymbol{T}^T_{\text{red2}}\boldsymbol{f}_{\text{DCB}}. \tag{34}$$

Vector $\boldsymbol{\eta}_{\text{DCBmod}}$ is the vector of modal coordinates of the system after the second reduction. The entire structure DOFs of Eq. (7) are finally approximated by

$$\begin{bmatrix}\boldsymbol{u}\\ \boldsymbol{\lambda}\end{bmatrix} \approx \boldsymbol{T}_{\text{DCB}}\boldsymbol{T}_{\text{red2}}\boldsymbol{\eta}_{\text{DCBmod}}. \tag{35}$$

After this second reduction, the modified DCBM reduced system has only positive eigenvalues. This makes a stable time integration possible.

If the first reduction basis $\boldsymbol{T}_{\text{DCB}}$ is enriched by an additional attachment mode as described in section 2.1.3, the steps of Eqs. (32) to (35) have to be executed with $\boldsymbol{T}_{\text{DCB,aug}}$ of Eq. (19) instead of $\boldsymbol{T}_{\text{DCB}}$. A corresponding reduction matrix $\boldsymbol{T}_{\text{red2}}$ is obtained. If this second reduction $\boldsymbol{T}_{\text{red2}}$ is then applied to the reduced system augmented by an additional attachment mode, the statically correct representation of the response to an external load is no longer guaranteed: parts of the subspace spanned by $\boldsymbol{T}_{\text{DCB,aug}}$ of Eq. (19) are truncated when applying the second reduction with basis $\boldsymbol{T}_{\text{red2}}$. This problem can once again be solved by enriching the reduction basis $\boldsymbol{T}_{\text{red2}}$. In this case, $\boldsymbol{T}_{\text{red2}}$ is enriched by the structure's static response $\boldsymbol{\psi}_a$ related to the point of application of the external force $\boldsymbol{f}$. The augmented second reduction matrix $\boldsymbol{T}_{\text{red2,aug}}$ results:

$$\boldsymbol{T}_{\text{red2,aug}} = \begin{bmatrix}\boldsymbol{T}_{\text{red2}} & \boldsymbol{\psi}_a\end{bmatrix} \tag{36}$$

With the reduction matrix $\boldsymbol{T}_{\text{red2,aug}}$ instead of $\boldsymbol{T}_{\text{red2}}$ in Eqs. (33) to (35) for the second reduction, we can perform a modal reduction to remove the effect of the negative eigenvalues without truncating the beneficial contribution of the additional attachment mode which was particularly added in Eq. (19).

3.2 Modal interface reduction of dual Craig-Bampton reduced system

Now only the interface problem of the DCBM reduced system is further reduced. The interface problem for the DCBM is obtained by static condensation of the dually assembled problem (7) on the interface degrees of freedom [19]. The interface DOFs are the amplitudes $\boldsymbol{\alpha} = \begin{bmatrix}\boldsymbol{\alpha}^{(1)} & \dots & \boldsymbol{\alpha}^{(N)}\end{bmatrix}^T$ of the rigid body modes of all substructures and the entire vector $\boldsymbol{\lambda}$ of Lagrange multipliers. This is equivalent to a DCBM reduction with no free vibration modes kept in the reduction basis $\boldsymbol{T}_{\text{DCB}}$ of Eq. (16). The modal interface reduction of DCBM reduced

systems [19] originally aimed to reduce the still significant size of interface DOFs of a DCBM reduced system rather than removing negative eigenvalues. The resulting mass and stiffness matrices of the interface problem are denoted as $\boldsymbol{M}_{\text{DCB,int}}$ and $\boldsymbol{K}_{\text{DCB,int}}$, respectively. The interface normal modes $\boldsymbol{x}_{\text{int},j}$ are the eigenvectors of the corresponding eigenproblem

$$\left(-\omega_{\text{int},j}^2 \boldsymbol{M}_{\text{DCB,int}} + \boldsymbol{K}_{\text{DCB,int}}\right) \boldsymbol{x}_{\text{int},j} = \boldsymbol{0}. \tag{37}$$

If only a certain number of interface normal modes $\boldsymbol{x}_{\text{int},j}$ is gathered as columns of matrix $\boldsymbol{X}_{\text{int}}$, the matrix $\boldsymbol{X}_{\text{int}}$ is used to approximate the interface DOFs $\boldsymbol{\alpha}$ and $\boldsymbol{\lambda}$:

$$\begin{bmatrix} \boldsymbol{\alpha} \\ \boldsymbol{\lambda} \end{bmatrix} \approx \boldsymbol{X}_{\text{int}} \tilde{\boldsymbol{\lambda}} \tag{38}$$

Vector $\tilde{\boldsymbol{\lambda}}$ contains the amplitudes $\tilde{\lambda}_j$ of the retained interface modes $\boldsymbol{x}_{\text{int},j}$. If the DCBM reduction of Eq. (17) is performed first, the modal parameters $\boldsymbol{\eta} = \begin{bmatrix} \boldsymbol{\eta}^{(1)} & \dots & \boldsymbol{\eta}^{(N)} \end{bmatrix}^T$ of all substructures are not affected by the interface approximation of Eq. (38).

To remove the negative eigenvalues from the DCBM reduced system (17), only the eigenvectors $\boldsymbol{x}_{\text{int},j}$ corresponding to positive eigenvalues $\omega_{\text{int},j}^2$ of the interface eigenproblem (37) are kept in the matrix $\boldsymbol{X}_{\text{int}}$. Subsequently, the interface reduction (38) is applied. $\boldsymbol{X}_{\text{int}}$ can be used to construct a related reduction matrix $\boldsymbol{T}_{\text{red2}}$, which allows one to express the modal interface reduction by Eqs. (33) to (35). For further details concerning interface reduction procedures of DCBM reduced systems see [19, 20]. The final modified DCBM system does not have any negative eigenvalues anymore. This also allows for a stable time integration.

4 NUMERICAL EXAMPLE

The two-dimensional structure of Figure 2 is considered for a numerical evaluation of the proposed time integration strategies. The structure is clamped on the left side in both directions

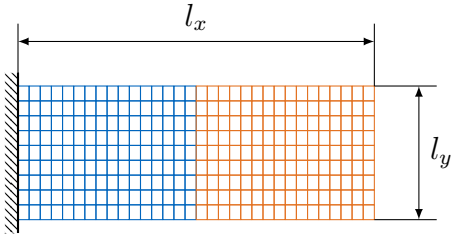

Figure 2: Two-dimensional solid problem (width $l_x = 8.0\,\text{cm}$, height $l_y = 3.0\,\text{cm}$, depth $l_z = 1.0\,\text{cm}$) clamped on the left side in both directions and decomposed into two substructures (indicated by different colors). Each substructure is discretized by 16×9 bilinear four-noded elements (plane stress, Young's modulus $E = 2.1 \cdot 10^{11}\,\text{N}\,\text{m}^{-2}$, density $\rho = 7.8 \cdot 10^3\,\text{kg}\,\text{m}^{-3}$). Stiffness proportional viscous damping $\boldsymbol{C} = a_1 \boldsymbol{K}$ is assumed with proportional factor $a_1 = \frac{2\xi_1}{\omega_1}$ with modal damping $\xi_1 = 0.1\,\%$ for the lowest eigenfrequency $\omega_1 = 362.7\,\text{Hz}$.

and decomposed into two substructures (indicated by different colors in Figure 2). Each substructure is discretized by 16×9 bilinear four-noded elements (plane stress). This results in 660 DOFs in the assembled unreduced displacement vector $\boldsymbol{u}$ and $n_\lambda = 20$ Lagrange multipliers resulting in a total number of $n_{total} = 680$ DOFs of Eq. (7). To compare the results, the unreduced system and a reduced system obtained by a Craig-Bampton reduction (CBM) are also

simulated. With 20 normal modes per substructure the CBM reduction provides a reduced system with $n_{\text{CB}} = 60$ DOFs, and the DCBM reduced system has $n_{\text{DCB}} = 63$ DOFs. Thereby, the DCBM reduced system has 20 negative eigenvalues. Therefore, stable DCBM reduced systems resulting from either a second modal reduction (see section 3.1) or a modal interface reduction (see section 3.2) have 43 remaining DOFs after removing the negative eigenvalues. Two load cases are exemplarily considered in the following:

- **Free vibration after static initial displacement**. The system of Figure 2 is loaded by a static force f_0 at the upper-right corner as depicted in Figure 3a. This causes the static deformation illustrated in Figure 1a. The initially prestressed structure of Figure 1a is released without initial velocity. No further external forces act on the structure over time. The vertical displacement u_{ur} of the upper-right corner is considered for free vibration.
- **Sinusoidal force excitation**. The system of Figure 2 is loaded by a sinusoidal force $f(t) = \hat{f}_0 \sin(\Omega t)$ with excitation frequency Ω at the upper-right corner as depicted in Figure 3b. The vertical displacement u_{ur} of the upper-right corner is considered and the frequency response function (FRF) is computed.

(a) Structure loaded by static force f_0.

(b) Structure loaded by sinusoidal excitation $f(t) = \hat{f}_0 \sin(\Omega t)$.

Figure 3: External forces applied to the two-dimensional solid problem of Figure 2.

4.1 Free vibration after static initial displacement

First, free vibration of the substructured system of Figure 2 is considered. The system is released from the initial displacement $\boldsymbol{u}_0$ depicted in Figure 1a without an initial velocity, i.e., $\dot{\boldsymbol{u}}_0 = \boldsymbol{0}$. The initial displacement $\boldsymbol{u}_0$ is the static deformation due to a vertical static force $f_0 = 1\,\text{kN}$ at the upper-right corner as illustrated by Figure 3a. First of all, $\boldsymbol{u}_0$ is computed by solving Eq. (39) with the stiffness matrix $\boldsymbol{K}$ of the assembled unreduced system of Figure 2:

$$\boldsymbol{u}_0 = \boldsymbol{K}^{-1}\boldsymbol{f}_0 \qquad \text{with} \qquad \boldsymbol{f}_0 = \begin{bmatrix} 0 \\ \vdots \\ 0 \\ f_0 \end{bmatrix} \tag{39}$$

Thereby, it is assumed in Eq. (39) that the point of application of force f_0 corresponds to the last degree of freedom in the displacement vector $\boldsymbol{u}_0$. In general, the row entry of the static force f_0 in the static force vector $\boldsymbol{f}_0$ corresponds to the displacement degree of freedom related to the point of application of the force f_0. The initial condition $\boldsymbol{u}_{\text{red2},0}$ for the reduced systems is obtained by solving

$$\boldsymbol{K}_{\text{red2}}\boldsymbol{u}_{\text{red2},0} = \boldsymbol{f}_{\text{red2}} \qquad \text{with} \qquad \boldsymbol{f}_{\text{red2}} = \boldsymbol{T}_{\text{red2}}^T\boldsymbol{T}_{\text{red1}}^T\boldsymbol{f}_0. \tag{40}$$

The force vector $\boldsymbol{f}_0$ is first projected onto the respective reduction basis to obtain the force vector $\boldsymbol{f}_{\text{red2}}$ in reduced coordinates and then the linear static problem is solved. For instance, if no additional attachment modes are used and a DCBM reduction with a subsequent modal reduction is performed, then $\boldsymbol{T}_{\text{red1}}$ is equal to $\boldsymbol{T}_{\text{DCB}}$ of Eq. (16) and $\boldsymbol{T}_{\text{red2}}$ is the second reduction matrix derived in section 3.1.

Figure 4 shows the vertical displacement u_{ur} of the upper-right corner after releasing the structure from the initial displacement $\boldsymbol{u}_0$. The displacement u_{ur} is depicted for the unreduced system, the CBM reduced system, the DCBM reduced system with subsequent modal reduction, and the DCBM reduced system with modal interface reduction. The first important observation

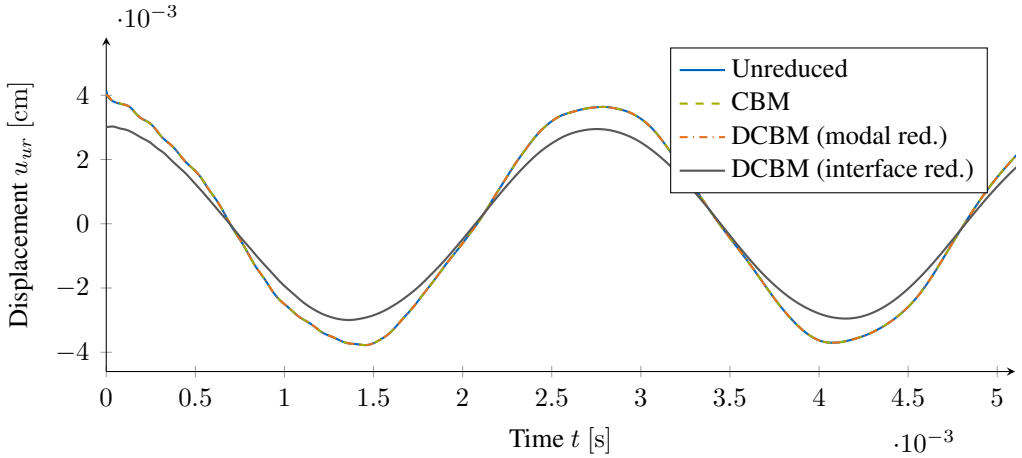

Figure 4: Vertical displacement u_{ur} of the upper-right corner for unreduced system, CBM reduction, DCBM reduction with subsequent modal reduction and DCBM reduction with interface reduction. The structure is released from the initial displacement $\boldsymbol{u}_0$ depicted in Figure 1a without an initial velocity.

is that the time integration is stable for all methods. However, the DCBM system with interface reduction fails to approximate the displacement of the unreduced system properly. This seems consistent with the results obtained in [20]. There it was shown that the modal interface reduction works well if some negative eigenvalues are kept, but struggles to approximate the eigenfrequencies if all modes corresponding to negative eigenvalues ω^2 are removed. The displacements of the unreduced, the CBM reduced and the DCBM system with subsequent modal reduction seem to coincide in Figure 4. The subsequent modal reduction of the DCBM reduced system for removing negative eigenvalues seems to be very promising compared to the modal interface reduction of the DCBM reduced system. Therefore, only DCBM reduced systems with subsequent modal reduction are investigated in detail in the following.

Now the representation of the initial deformation of Figure 1a is considered, which corresponds to time $t = 0$ in Figure 4. The first time steps ($t < 0.1 \cdot 10^{-3}$ s) of the motion are plotted in Figure 5a. There is a noticeable difference between the initial displacement of the unreduced system, the CBM and DCBM reduced systems. This is a result of the reduction bases not being able to represent the static deformation $\boldsymbol{u}_0$, which is caused by force f_0 at the upper-right corner, correctly. To encounter this discrepancy for the initial condition, the addition of a static mode representing the static deformation caused by the external force applied to the system is employed, as proposed in section 2.1.3. Consequently, the augmented reduction matrix $\boldsymbol{T}_{\text{red2,aug}}$ of Eq. (36) is used instead of $\boldsymbol{T}_{\text{red2}}$ as exhibited in section 3.1 for the DCBM reduction. The same is done for the CBM reduction basis. Therefore, both the CBM and the DCBM reduced

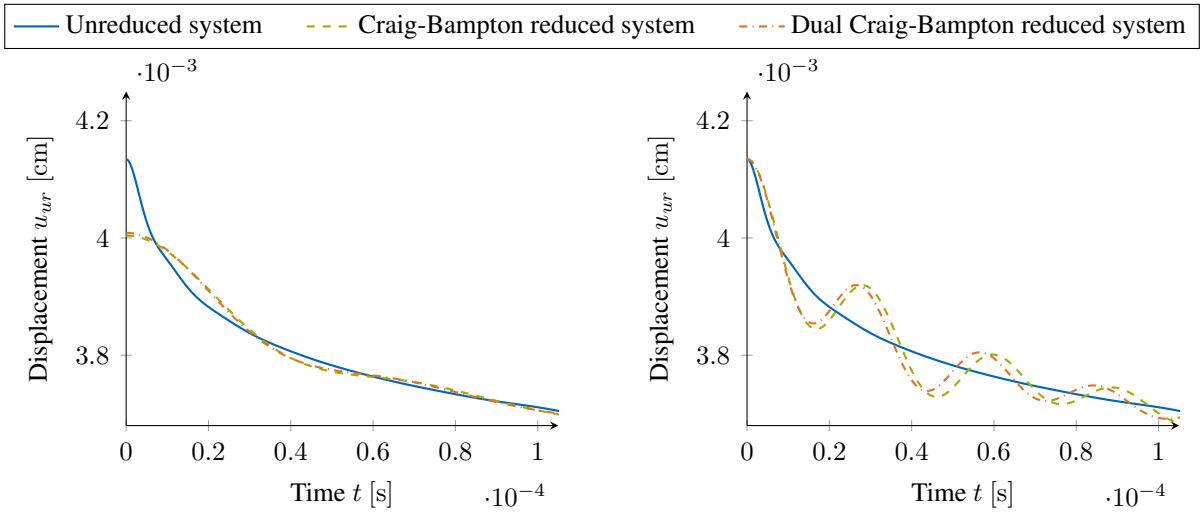

(a) Reduced systems without additional attachment mode related to the point of application of force f_0.

(b) Reduced systems with additional attachment mode related to the point of application of force f_0.

Figure 5: Vertical displacement u_{ur} of the upper-right corner for $t < 0.1 \cdot 10^{-3}$ s for unreduced system, CBM reduction and DCBM reduction with subsequent modal reduction. The structure is released from the initial displacement $\boldsymbol{u}_0$ depicted in Figure 1a without an initial velocity.

system are able to represent the correct initial displacement $\boldsymbol{u}_0$. This is shown for the vertical displacement u_{ur} of the upper-right corner in Figure 5b for time $t = 0$: u_{ur} of the reduced systems coincides with the unreduced system.

The positive effect of the additional mode is obvious, but there is also a spurious oscillation in both reduced systems related to this additional mode. Note that for this example stiffness proportional viscous damping $\boldsymbol{C} = a_1 \boldsymbol{K}$ is assumed (see caption of Figure 2 for details). Figure 6 shows the displacement u_{ur} of the upper-right corner for a larger time period. At the very

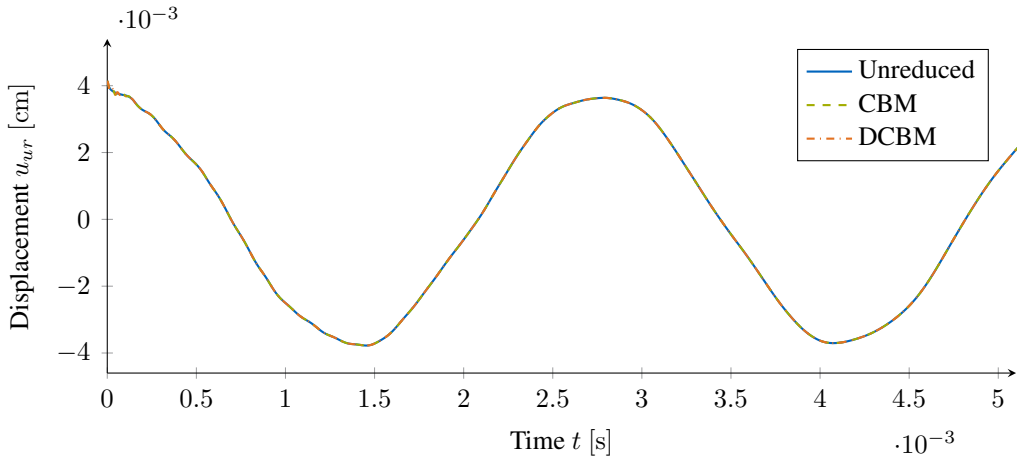

Figure 6: Vertical displacement u_{ur} of the upper-right corner for unreduced system, CBM reduction and DCBM reduction with subsequent modal reduction with additional attachment mode related to the point of application of force f_0. The structure is released from the initial displacement $\boldsymbol{u}_0$ depicted in Figure 1a without an initial velocity.

beginning ($t < 0.1 \cdot 10^{-3}\,\mathrm{s}$), the oscillation of Figure 5b is noticeable, but subsides very fast. Nonetheless, this spurious oscillation will not disappear if the underlying system is not damped. The usage of the generalized-α method [21] instead of Newmark's method to introduce numerical damping can suppress this high frequency part of the solution.

To conclude, the additional attachment mode fulfills its purpose regarding the initial state, but has an undesired oscillatory effect during the first time steps. If there is little damping, this oscillation will die out after a few time steps and does not have any negative influence on the approximation accuracy over time.

4.2 Sinusoidal excitation

For further investigations, the structure is loaded to a sinusoidal excitation. As depicted in Figure 3b, the sinusoidal force

$$f(t) = \hat{f}_0 \sin(\Omega t) \tag{41}$$

with excitation frequency Ω acts at the upper-right node (equal to the static force in the previous section). The initial conditions for displacements $\boldsymbol{u}_0$ and velocities $\dot{\boldsymbol{u}}_0$ are

$$\boldsymbol{u}_0 = \dot{\boldsymbol{u}}_0 = \boldsymbol{0}. \tag{42}$$

First, the transient behavior of the system is investigated in time domain and, afterwards, the frequency response functions (FRFs) for the vertical displacement of the upper-right corner are considered.

4.2.1 Time domain

The system's behavior in time domain is now considered. Amplitude $\hat{f}_0 = 1\,\mathrm{kN}$ and excitation frequency $\Omega = 2500\,\mathrm{Hz}$ are prescribed, i.e., the excitation frequency Ω lies in the middle of the third and fourth eigenfrequencies of the system. Note that the second eigenfrequency of the systems corresponds to the first longitudinal mode.

The vertical displacement u_{ur} of the upper-right corner is shown due to sinusoidal load in Figure 7: The graphs in Figure 7a are obtained when no additional attachment mode is added to the reduced systems. The first important observation is that the time integration is again stable. Nevertheless, large discrepancies occur between the displacements of the unreduced and reduced systems: the displacements of the unreduced system are very roughly followed by those of the reduced systems, but the values at a certain time do not particularly match.

For that reason, the bases of the reduced systems are augmented by a static mode as described in sections 2.1.3 and 3.1. If an additional attachment mode related to the point of application of force $f(t)$ is added to the reduced systems, the graphs in Figure 7b result. The effect of the additional mode is eminently significant in this case. The displacements of the reduced systems coincide now with those of the unreduced system. No discrepancy is noticeable.

To stress this, Figure 8 depicts the vertical displacement u_{ur} of the upper-right corner for a later time interval ($8.8 \cdot 10^{-2}\,\mathrm{s} < t < 9.2 \cdot 10^{-2}\,\mathrm{s}$). Again, the displacements of the unreduced and reduced systems coincide if the additional attachment mode related to the point of application of force $f(t)$ is added (Figure 8b). Figure 8a clearly illustrates that the displacements of the reduced systems roughly follow those of the unreduced system. The displacements of the reduced systems without additional attachment mode seem to be a kind of mean value of the displacements of the unreduced system. However, the approximation of the displacement u_{ur} at a certain time is poor if no additional attachment mode related to the point of application of the external force is used.

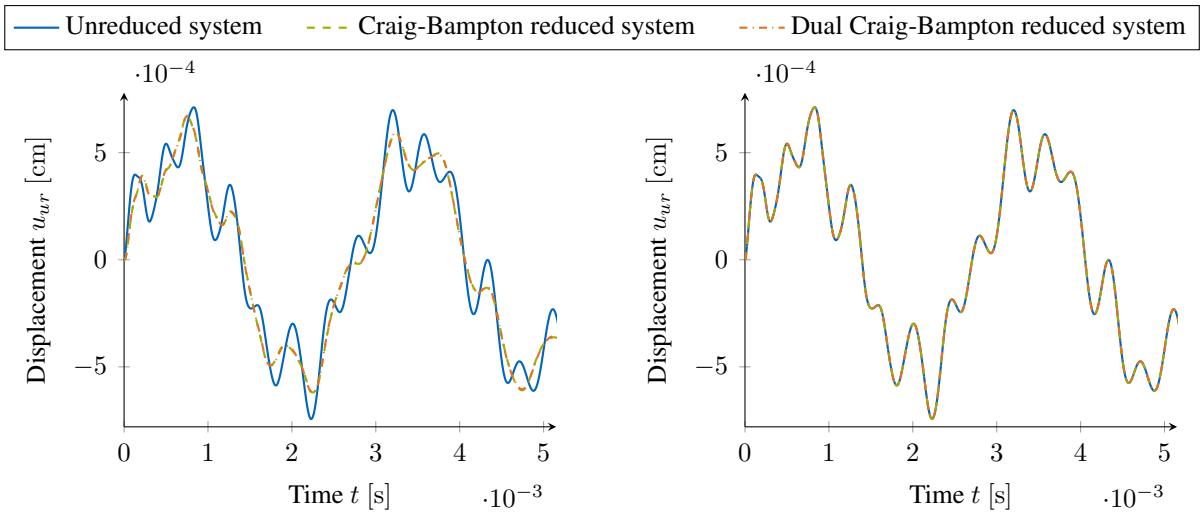

(a) Reduced systems without additional attachment mode related to the point of application of force $f(t)$.

(b) Reduced systems with additional attachment mode related to the point of application of force $f(t)$.

Figure 7: Vertical displacement u_{ur} of the upper-right corner for unreduced system, CBM reduction and DCBM reduction with subsequent modal reduction. The structure has no initial displacement and no initial velocity $\boldsymbol{u}_0 = \dot{\boldsymbol{u}}_0 = \mathbf{0}$ and is excited by a sinusoidal load $f(t) = \hat{f}_0 \sin(\Omega t)$ as depicted in Figure 3b. Amplitude $\hat{f}_0 = 1\,\mathrm{kN}$ and excitation frequency $\Omega = 2500\,\mathrm{Hz}$ are prescribed.

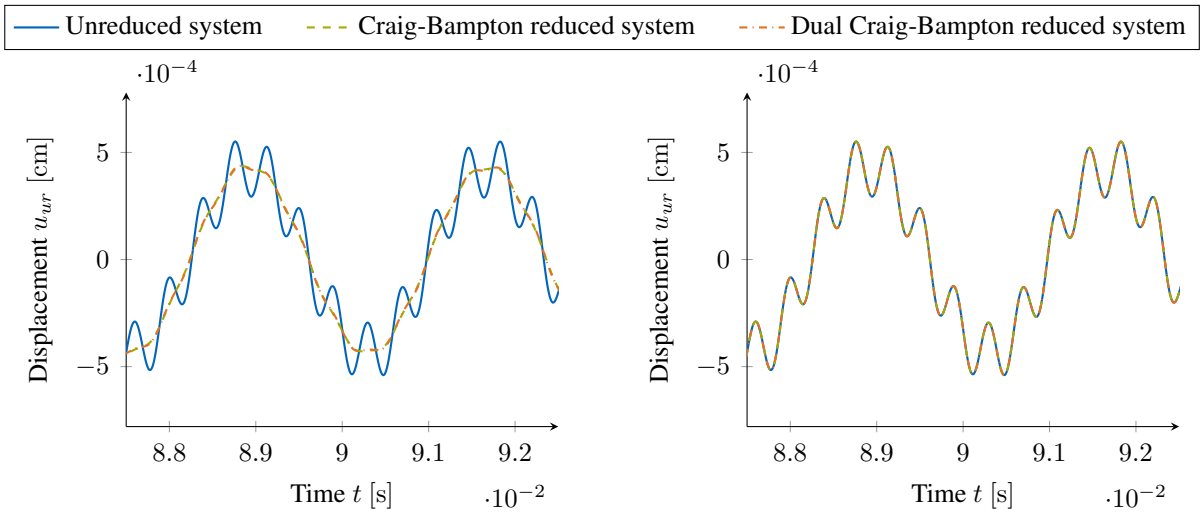

(a) Reduced systems without additional attachment mode related to the point of application of force $f(t)$.

(b) Reduced systems with additional attachment mode related to the point of application of force $f(t)$.

Figure 8: Vertical displacement u_{ur} of the upper-right corner for $8.8 \cdot 10^{-2}\,\mathrm{s} < t < 9.2 \cdot 10^{-2}\,\mathrm{s}$ for unreduced system, CBM reduction and DCBM reduction with subsequent modal reduction. The structure has no initial displacement and no initial velocity $\boldsymbol{u}_0 = \dot{\boldsymbol{u}}_0 = \mathbf{0}$ and is excited by a sinusoidal load $f(t) = \hat{f}_0 \sin(\Omega t)$ as depicted in Figure 3b. Amplitude $\hat{f}_0 = 1\,\mathrm{kN}$ and excitation frequency $\Omega = 2500\,\mathrm{Hz}$ are prescribed.

4.2.2 Frequency domain

To further assess the approximation accuracy of the DCBM reduced system with subsequent modal reduction, the system's behavior is now considered for varying excitation frequencies Ω. Therefore, the frequency response function (FRF) is computed for the driving point, i.e., the amplitude $\hat{u}_{ur}$ of the vertical displacement u_{ur} of the upper-right corner due to the vertical sinusoidal force $f(t) = \hat{f}_0 \sin(\Omega t)$ at this node (see Figure 3b). Figure 9 shows the FRFs for the unreduced and reduced systems if a force amplitude $\hat{f}_0 = 1\,\mathrm{kN}$ is prescribed.

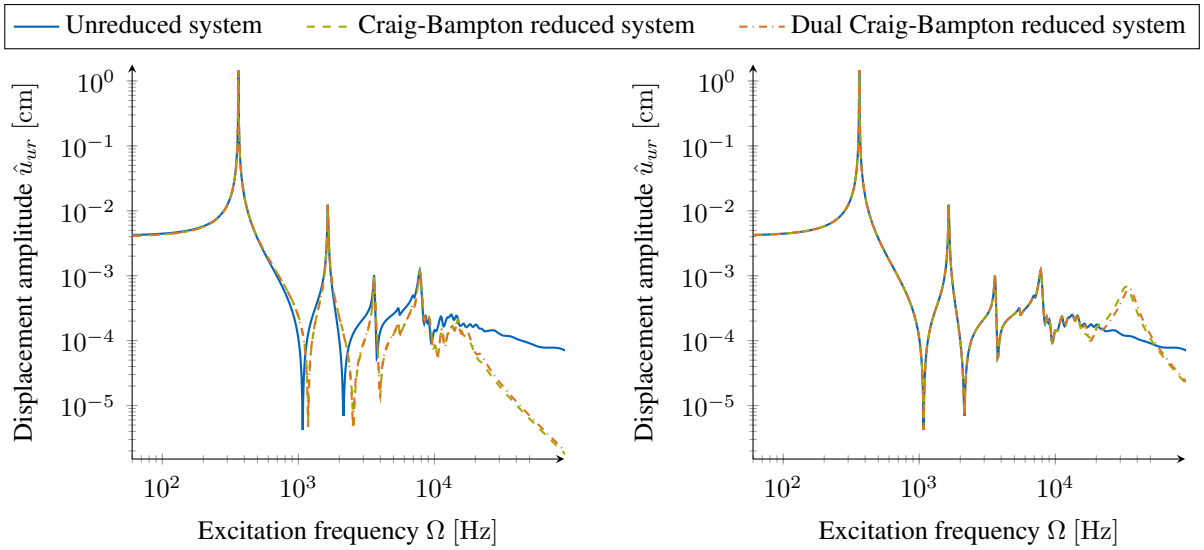

(a) Reduced systems without additional attachment mode related to the point of application of force $f(t)$.

(b) Reduced systems with additional attachment mode related to the point of application of force $f(t)$.

Figure 9: Amplitude $\hat{u}_{ur}$ of vertical displacement u_{ur} of the upper-right corner for unreduced system, CBM reduction and DCBM reduction with subsequent modal reduction. The structure is excited by a sinusoidal load $f(t) = \hat{f}_0 \sin(\Omega t)$ as depicted in Figure 3b. Force amplitude $\hat{f}_0 = 1\,\mathrm{kN}$ is prescribed and stiffness proportional viscous damping $\boldsymbol{C} = a_1 \boldsymbol{K}$ is assumed (see caption of Figure 2 for details).

Thereby, the FRFs are plotted for the reduced systems without an additional attachment mode in Figure 9a. The resonance peaks coincide for the unreduced and reduced systems, but significant differences occur in between the resonance peaks. The antiresonances are especially poorly fitted.

In addition to that, the FRFs are depicted for the reduced systems with an additional attachment mode in Figure 9b. For $\Omega < 15\,\mathrm{kHz}$, the graphs coincide again. Both resonances and antiresonances are hit very well. As expected for reduced systems, deviations show up only in the high frequency range. The most noticeable difference is the broad peak (maximum at around $\Omega \approx 33\,\mathrm{kHz}$) introduced by the additional attachment mode. This peaks shows up for both the CBM reduced system and the DCBM reduced system. Therefore, the amplitudes near that frequency are overestimated by the reduced systems.

This does not matter so much if there is little material damping in the system. In this example, stiffness proportional viscous damping $\boldsymbol{C} = a_1 \boldsymbol{K}$ is assumed with proportional factor $a_1 = \frac{2\xi_1}{\omega_1}$ with modal damping $\xi_1 = 0.1\,\%$ for the lowest eigenfrequency $\omega_1 = 362.7\,\mathrm{Hz}$. As Figures 6, 7

and 8 indicate for the slightly damped system considered here, the displacements of the reduced systems coincide with the displacements of the unreduced system. Hence, the peak at around $\Omega \approx 33\,\mathrm{kHz}$ introduced by the additional attachment mode in the FRF in Figure 9b does not deteriorate the excellent approximation in time domain.

Now the simulations are repeated unmodified with the same conditions as in Figure 7b except that an undamped system is assumed (viscous damping matrix $\boldsymbol{C} = \boldsymbol{0}$). Figure 10 shows the vertical displacement u_{ur} of the upper-right corner for an underlying system with no damping. At first glance, the displacements seem to coincide with a certain tolerance in Figure 10a, but

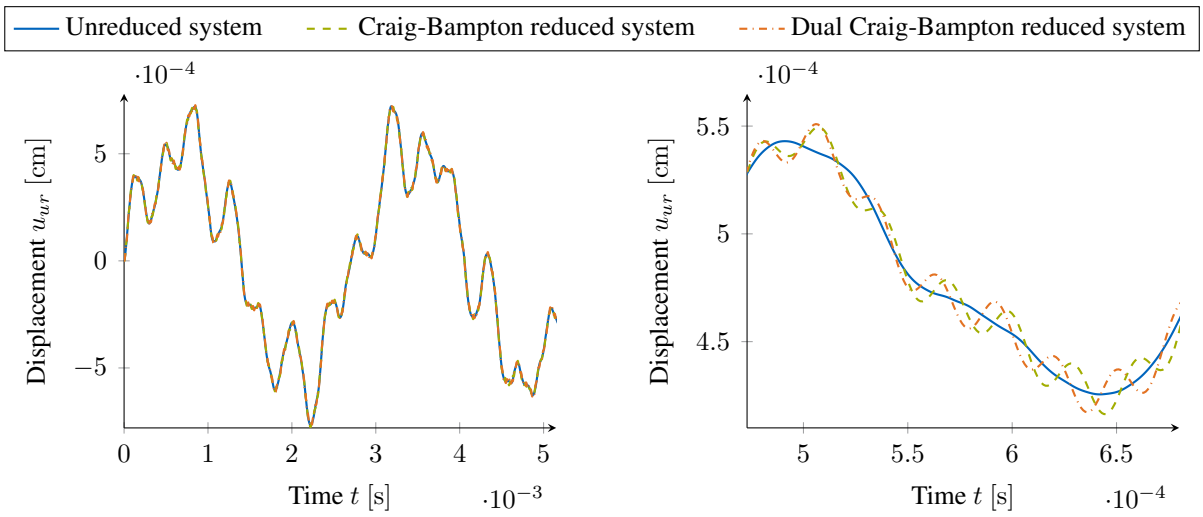

(a) Reduced systems with additional attachment mode related to the point of application of force $f(t)$.

(b) Zoom plot of Figure 10a in time interval $0.47 \cdot 10^{-3}\,\mathrm{s} < t < 0.68 \cdot 10^{-3}\,\mathrm{s}$.

Figure 10: Vertical displacement u_{ur} of the upper-right corner for unreduced system, CBM reduction and DCBM reduction with subsequent modal reduction. The same conditions as in Figure 7b are taken except that an undamped system is assumed (viscous damping matrix $\boldsymbol{C} = \boldsymbol{0}$).

also small deviations are identifiable. The zoom plot in Figure 10b shows that in detail. The reduced systems introduce an oscillation with a high frequency on top of the motion of the unreduced system. The period of that high frequency oscillation corresponds to the peak at around $\Omega \approx 33\,\mathrm{kHz}$ in the FRFs of the reduced systems in Figure 9b. As already mentioned, this peak is a result of the additional attachment mode related to the point of application of the external force.

To draw a conclusion, the additional attachment mode has a significant beneficial contribution to the approximation accuracy of the solution if the system is slightly damped: the displacements over time match entirely for unreduced and reduced systems (see Figure 7b and 8b) and, moreover, all resonances and antiresonances coincide up to a certain cut-off frequency (see Figure 9b). An additional peak in the FRFs is introduced by the additional attachment mode (Figure 9b). If the system is slightly damped, the approximation quality is not influenced by this additional peak. But if an undamped system is assumed, a high frequency oscillation occurs. On the one hand, this can be weakened by choosing a higher reduced order, which shifts the peak towards higher frequencies. On the other hand, the generalized-α method [21] can remedy by introducing numerical damping.

5 RECOMMENDATIONS FOR TIME INTEGRATION OF DUAL CRAIG-BAMPTON REDUCED SYSTEMS

As a consequence of the results of the previous section, general recommendations shall now be given for a reliable time integration of dual Craig-Bampton (DCBM) reduced systems.

First of all, removing the negative eigenvalues of DCBM reduced systems yields time integration stable: modal interface reduction of the DCBM reduced systems makes the system stable, but the approximation is very inaccurate (see Figure 4). On the opposite, a subsequent modal reduction of the DCBM reduced system makes the reduced system also stable and provides accurate results. Both methods allow for stable time integration, but a subsequent modal reduction of the DCBM reduced systems is highly recommended as the method of choice.

Additional attachment modes related to the points of application of external forces are very beneficial if the system is slightly damped: displacements over time match entirely for unreduced and reduced systems (see Figures 6, 7b and 8b) and, moreover, all resonances and antiresonances coincide up to certain cut-off frequency (see Figure 9b). An additional peak in the FRFs is introduced by each additional attachment mode (see Figure 9b), which does not influence the approximation quality in time domain if the system is slightly damped (see Figures 6, 7b and 8b). Hence, if the points of application of external forces are known, it is also highly recommended to include additional static modes (which are attachment modes) related to the points of application of the forces in the reduction basis. This also guarantees the results to be static correct in any case (see Figure 5). To sum up, the excellent approximation quality is not influenced by this additional peak if the system is slightly damped.

But if an undamped system is assumed, a high frequency oscillation occurs (see Figure 10). On the one hand, this can be weakened by choosing a higher reduced order, which shifts the peak towards higher frequencies. On the other hand, generalized-α method can remedy by introducing numerical damping.

6 CONCLUSIONS

In this paper, the feasibility of a reliable time integration of dual Craig-Bampton (DCBM) reduced systems was demonstrated and investigated in detail. The principal unstable behavior of DCBM reduced systems can be overcome by two approaches: modal analysis of the DCBM reduced system as a subsequent step to the DCBM reduction or modal interface reduction during the DCBM reduction process.

The modal interface reduction is performed during the DCBM reduction process and only interface modes corresponding to positive eigenvalues are kept, resulting in a stable reduced system. Stable time integration is then indeed possible, but the approximation accuracy is poor.

Modal analysis of the DCBM reduced system as a subsequent step to the DCBM reduction leads to a stable reduced system and very accurate approximation results. Thereby, excellent accordance with the behavior of the unreduced system is obtained. Especially if attachment modes related to the points of application of external forces are added to the reduction basis, no noticeable differences occur between the unreduced and the DCBM reduced systems with subsequent modal reduction in the cases being considered. Consequently, this approach achieves high approximation accuracy and is therefore particularly appropriate for the time integration of dual Craig-Bampton reduced systems.

REFERENCES

[1] R. R. Craig and M. C. C. Bampton. “Coupling of Substructures for Dynamic Analyses”. In: *AIAA Journal* 6.7 (July 1968), pp. 1313–1319. DOI: 10.2514/3.4741.

[2] R. H. MacNeal. “A hybrid method of component mode synthesis”. In: *Computers and Structures* 1.4 (1971), pp. 581–601. DOI: 10.1016/0045-7949(71)90031-9.

[3] S. Rubin. “Improved Component-Mode Representation for Structural Dynamic Analysis”. In: *AIAA Journal* 13.8 (1975), pp. 995–1006. DOI: 10.2514/3.60497.

[4] R. R. Craig and C.-J. Chang. “On the use of attachment modes in substructure coupling for dynamic analysis”. In: *18th Structural Dynamics and Materials Conference*. Structures, Structural Dynamics, and Materials and Co-located Conferences. San Diego, CA, USA: American Institute of Aeronautics and Astronautics, Mar. 1977, pp. 89–99. DOI: doi:10.2514/6.1977-405.

[5] R. R. Craig. “Coupling of substructures for dynamic analyses: An overview”. In: *Proceedings of AIAA/ASME/ASCE/AHS/ASC structures, structural dynamics, and materials conference and exhibit*. Atlanta, GA, USA, 2000, pp. 1573–1584.

[6] D. J. Rixen. “A dual Craig-Bampton method for dynamic substructuring”. In: *Journal of Computational and Applied Mathematics* 168.1-2 (2004), pp. 383–391. DOI: 10.1016/j.cam.2003.12.014.

[7] R. R. Craig and A. J. Kurdila. *Fundamentals of structural dynamics*. John Wiley & Sons, 2006.

[8] S. N. Voormeeren, P. L. C. van der Valk, and D. J. Rixen. “Generalized Methodology for Assembly and Reduction of Component Models for Dynamic Substructuring”. In: *AIAA Journal* 49.5 (2011), pp. 1010–1020. DOI: 10.2514/1.J050724.

[9] F. M. Gruber and D. J. Rixen. “Evaluation of Substructure Reduction Techniques with Fixed and Free Interfaces”. In: *Strojniški vestnik - Journal of Mechanical Engineering* 62.7-8 (2016), pp. 452–462. DOI: 10.5545/sv-jme.2016.3735.

[10] F. M. Gruber, J. B. Rutzmoser, and D. J. Rixen. “Comparison between primal and dual Craig-Bampton substructure reduction techniques”. In: *Proceedings of the 11th International Conference on Engineering Vibration, Ljubljana, Slovenia*. Ed. by M. Boltezar, J. Slavic, and M. Wiercigroch. Ljubljana, Slovenia, 2015, pp. 1245–1254.

[11] M. Géradin and D. J. Rixen. *Mechanical vibrations: theory and application to structural dynamics*. John Wiley & Sons, 2015.

[12] D. J. Rixen. “Dual Craig-Bampton with enrichment to avoid spurious modes”. In: *Proceedings of IMAC-XXVII* (2009).

[13] E. L. Wilson, M.-W. Yuan, and J. M. Dickens. “Dynamic analysis by direct superposition of Ritz vectors”. In: *Earthquake Engineering & Structural Dynamics* 10.6 (Nov. 1982), pp. 813–821. DOI: 10.1002/eqe.4290100606.

[14] P. Léger and E. Wilson. “Generation of load dependent Ritz transformation vectors in structural dynamics”. In: *Engineering Computations* 4.4 (Apr. 1987), pp. 309–318. DOI: 10.1108/eb023709.

[15] P. Léger. “Load dependent subspace reduction methods for structural dynamic computations”. In: *Computers & Structures* 29.6 (1988), pp. 993–999. DOI: 10.1016/0045-7949(88)90325-2.

[16] J. Dickens and K. Pool. “Modal truncation vectors and periodic time domain analysis applied to a cyclic symmetry structure”. In: *Computers & Structures* 45.4 (Nov. 1992), pp. 685–696. DOI: 10.1016/0045-7949(92)90487-K.

[17] J. Dickens and A. Stroeve. “Modal truncation vectors for reduced dynamic substructure models”. In: *41st Structures, Structural Dynamics, and Materials Conference and Exhibit*. Reston, Virigina: American Institute of Aeronautics and Astronautics, Apr. 2000. DOI: 10.2514/6.2000-1578.

[18] N. M. Newmark. “A method of computation for structural dynamics”. In: *Journal of the engineering mechanics division* 85.3 (1959), pp. 67–94.

[19] D. J. Rixen. “Interface Reduction in the Dual Craig-Bampton method based on dual interface modes”. In: *Linking Models and Experiments, Volume 2: Proceedings of the 29th IMAC, A Conference on Structural Dynamics, 2011*. Ed. by T. Proulx. New York, NY: Springer New York, 2011, pp. 311–328. DOI: 10.1007/978-1-4419-9305-2_22.

[20] F. M. Gruber, T. L. Bürchner, and D. J. Rixen. “Dual Craig-Bampton Method with Reduction of Interface Coordinates”. In: *Proceedings of the 35th IMAC, A Conference and Exposition on Structural Dynamics 2017*. Springer International Publishing, 2017.

[21] J. Chung and G. M. Hulbert. “A Time Integration Algorithm for Structural Dynamics With Improved Numerical Dissipation: The Generalized-α Method”. In: *Journal of Applied Mechanics* 60.2 (June 1993), pp. 371–375. DOI: 10.1115/1.2900803.